Sky-Imager Forecasting for Improved Management of a Hybrid Photovoltaic-Diesel System

Olivier Liandrat*, Antonin Braun*, Étienne Buessler*, Marion Lafuma*,
Sylvain Cros*, André Gomez† and Louis-Étienne Boudreault*
*Reuniwatt SAS, 14 rue de la Guadeloupe, 97490 Sainte-Clothilde, France
†JA Delmas Caterpillar, 17 rue Vauban, 33075 Bordeaux Cedex, France

***Abstract*—The benefits of using forecasts for optimizing a hybrid PV-Diesel system are analyzed using a thermal-infrared sky-imager. A simple model of the hybrid mini-grid is designed to study the effect of the forecasts within different control scenarios of photovoltaic (PV) injection. When compared to a "no-forecast" scenario, the results suggest that including the forecasts can reduce the overall fuel consumption of the system while reducing the potential number of blackouts observed.**

I. Introduction

The worldwide increase in renewable energies leads to fundamental changes in power-grid management. In particular, for remote locations, photovoltaic (PV) energy represents potential benefits when used in combination with conventional standalone energy sources – such as diesel generators. Indeed, producing electricity from diesel in remote areas reveals truly expensive mainly due to the high fuel-transportation costs towards the isolated areas, supply risks (loss, theft, geopolitical context, etc.) and diesel-price fluctuations. The use of PV offers the opportunity to massively reduce the power-supply operating costs in offgrid systems. For decentralised industrial applications, such as in mining and agriculture, this represents a huge potential benefit. PV, used in combination with diesel gensets, can reduce the daytime fuel consumption by running the gensets at a partial load, or even by switching them off. Yet, a challenge arises as to achieve the highest possible solar penetration rate without risking a blackout, therefore requiring a careful monitoring of the forecoming sky-weather events. Indeed, the brutal drops of solar production caused by cloud movements must be compensated by ramping up the gensets in order to balance the demand load. On the other hand, running the gensets when the grid is overbalanced is regretful when the sunshine availability is high over a given day. Ground-based all-sky imagers capture a wide field of view of the sky, enabling to anticipate the forecoming cloud obstructions and therefore, the photovoltaic power fluctuations. They thus appear as a promising tool to manage the gensets spinning reserve according to the future available PV output.

Only a few number of studies exists in which sky-cam imagers are used to control the reponse of a hybrid PV-diesel system. Most of them used a so-called binary approach (clouds or no clouds) to alert their system of forecoming drops, either in the form of a general threshold using past information about clouds [1] or from forecasts built from the camera [2]. Sky-cam forecasts were also integrated into complete modelling systems [3], [4]. These studies however reported modest fuel consumption ($< 2\%$) at a PV penetration of about 30% of the peak load, perhaps related to their pessimistic forecast and power plant configurations.

In this study, we investigate the impact of the forecast onto the fuel consumption and the blackouts number of a simplified hybrid PV-diesel system. The model is simulated using a standard PV penetration of 30% and a constant load. The PV output is modelled using 1 min irradiance measurements from the pyranometer located at the site Le Portail (Latitude: $-21.22°$, Longitude: $55.30°$), on Reunion Island, France, with the forecasts delivered using a thermal-infrared sky-imager also present on this site.

Section II first details the hybrid system model, the thermal-infrared sky-imager, the hybrid system control and the performance metrics used to evaluate the simulations. Then, section III presents output results from the hybrid model in various system control scenarios, including those with and without forecasts. A discussion and a brief conclusion are finally given in section IV and section V, respectively.

II. Methodology

A. Hybrid PV-diesel model

As we seek to verify the effect of forecasts, a hybrid PV-diesel system assuming a constant demand load L is modelled. The system consists in two main components, namely diesel gensets delivering each a power $P_{gen}(t)$ and a PV system delivering a power $P_{PV}(t)$. The nominal powers of the hybrid system components are specified in Table I. The PV plant power is assumed varying as the sun availability as

$$P_{PV}(t) = P_{PV,nom} \cdot k_c(t), \tag{1}$$

where k_c is the clear sky index defined as

$$k_c(t) = \frac{GHI(t)}{GHI_{clearsky}(t)}, \tag{2}$$

where the PV system is assumed responding instantaneously to the solar irradiance. We also consider that the PV pannels are always operating at their maximum power point of current and voltage and have a perfect efficiency at the inverters output ($\eta_{PV} = 1$). The GHI is the global horizontal irradiance extracted from the pyranometer data

TABLE I
Nominal power of the hybrid system components

Demand load	Solar plant power	Gensets total power
L	$P_{PV,nom}$	$P_{gen,nom}$
3 MW	1 MW	15 units × 0.2 MW

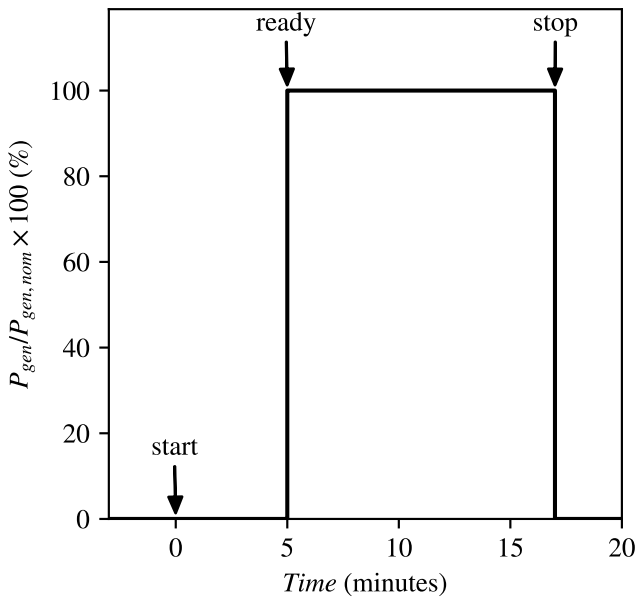

Fig. 1. Illustration of the functioning process of the modelled gensets. The gensets are (ready) delivering their ouput power 5 minutes after they have been ignited (start) and can be switched off instantaneously at any given time (stop).

and $GHI_{clearsky}$ is calculated using the ESRA clear sky model [9]. For the gensets, they reach their output power as

$$P_{gen}(t) = \begin{cases} 0 & \text{if } 0 < t < 5 \text{ mins (spin-up)}, \\ P_{gen,nom} & \text{if } t \geq 5 \text{ mins}, \end{cases} \tag{3}$$

where a genset is considered being operational only when it has finished its spin-up time of 5 minutes from a cold-start (see Fig. 1). Here, we consider that the gensets only operate at their nominal (or rated) power after they have been ignited ($P_{gen} = P_{gen,nom}$). The gensets are also considered ideal ($\eta_{gen} = 1$), meaning that they always operate at their output power without any losses.

Overall, the system is balanced as follows,

$$B(t) = P_{PV}(t) + \sum_{i=1}^{k} P_{gen,i}(t) - L, \tag{4}$$

with $B(t)$ being the load balance, L the total load on the system and k the number of gensets which are switched on at a given time t. The system is balanced if $B(t) \geq 0$, otherwise a blackout occurs ($B(t) < 0$).

B. Sky-imager forecasts

The *SkyInsight* is a multi-component imaging system with at its core a long-wave infrared thermal camera looking down onto an hemispherical convex mirror, thereby providing wide-angle images of the above sky-vault temperature at a constant framerate ($\Delta t = 1\,\text{min}$). The camera is featuring an uncooled micro-bolometer array of 382×288 pixels. Three other sensors equip the system, namely an ambient temperature sensor, a humidity sensor and an irradiance sensor. The system includes a mini-PC acting as a controlling unit for the image acquisition and for communication over network, from which the images are sent towards a remote server. The system also contains a relay card for the distant rebooting of the camera.

The forecast model from the imager involves a multi-step procedure. First, a geometric calibration using the position of the sun is performed to assign the pixels with zenith-azimuth angles. Second, a radiometric calibration procedure is applied to convert the raw pixels into luminance pixels. A background clear sky look-up table of luminance is then recovered from the images. A radiative transfer model inversion [5] is applied to tranform the background and cloud luminance into optical depth (OD) maps of the clouds. Once the OD maps are obtained, a number of features serving as a training dataset to a machine learning algorithm are calculated. The features include two types: image and dynamical features. The image features include the cloud fraction, the clear sky index and the weighted cloud fraction. The cloud fraction is obtained from cloud segmentation by applying a binary (cloud or no clouds) threshold on the optical depth. The dynamical features is a patch containing the image features of the size of the sun which is projected forward in time towards the sun at different horizons ($t \rightarrow t+10$ mins). The time projection is performed using a global motion vector calculated from one image to the other as the median of a vector field derived from an optical flow algorithm (the Farneback algorithm precisely [6]).

Random Forest Regression Trees [7] using a loss function to perform various levels of pessimistic predictions towards target quantiles are trained on a 3-month dataset of features and irradiance data. The next month's irradiance following the training is then forecasted at every timestep Δt up to an horizon of 10 minutes. More details about the methodology of the forecast procedure with the *Sky Insight* can be found in [8].

C. System control

For the system control, a total genset power target $P_{target}(t)$ is defined at each time step Δt. In the case where no forecasts are used, P_{target} is set as the current power that would be needed to achieve the balance if only a fraction α of the current PV power was available, i.e.

No forecasts:

$$P_{target}(t) = L - \alpha \cdot P_{PV}(t), \tag{5}$$

where α can be adjusted between [0,1]. In the case where the solar forecasting is used, P_{target} is set in order to achieve the balance with the lowest forecasted PV power available within the next 10 minutes $P_{PV,min}$ as

With forecasts:

$$P_{target}(t) = L - P_{PV,min}(t \rightarrow t + 10 \text{ mins}). \tag{6}$$

In addition to the quantile forecasts provided by the sky-imager, $P_{PV,min}$ was also introduced a "perfect forecast" directly built from the measured minimum PV output within the next 10 mins. Once $P_{target}(t)$ is computed, gensets start or stop commands are sent to the system in order to reach the power target with a minimun number of gensets needed. This is achieved by looping trough all n gensets of the system in

(a)

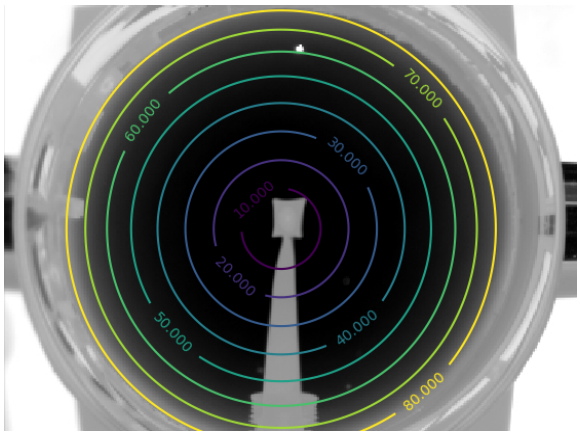

(b)

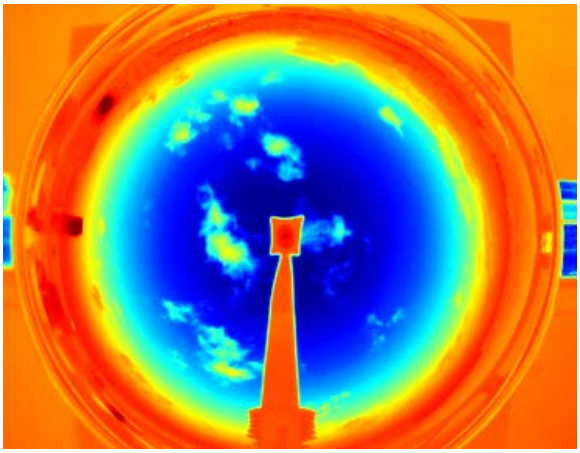

(c)

Fig. 2. (a) The *Sky Insight* thermal-infrared sky-imager system at the site Le Portail, (b) geometric calibration showing the zenithal angles on the image and (c) thermographic image with clouds showed as warmer patches superimposed on the cooler clear sky background.

a fixed order, from genset number $i = 1$ to genset number $i = k$. Let $P_{gen}(k) = \sum_{i=1}^{k} P_{gen,nom}$ be the power available with k gensets ready. We look at the minimum k for which $P_{gen}(k) \geq P_{target}(t)$, we fix $k_0 = k$ for this $P_{gen}(k)$ and then, the following commands are sent to the gensets:

1) every genset i where $k \leq k_0$ are switched on (if not already on) and,
2) every genset i where $k > k_0$ are switched off (if not already off).

This process is repeated at every time steps.

D. Performance metrics

In the following results, several performance metrics are calculated. Namely, the load balance error is defined as

$$Load\ balance\ error = \frac{\sum_{t=0}^{\infty} B(t)\Delta t}{\sum_{t=0}^{\infty} L(t)\Delta t}, \tag{7}$$

and the energy consumption (in kWh) is defined as

$$E_{tot} = \sum_{t=0}^{\infty} P_{gen,tot}(t)\Delta t. \tag{8}$$

To compare the energy savings with a reference case, the case where $\alpha = 0$ is used. This case corresponds to the case as if no PV power was used and only the gensets were providing all the needed power. If we let energy saving be equal to the genset fuel saving, the fuel reduction can defined as

$$Fuel\ reduction = \frac{E_{tot} - E_{tot,ref}}{E_{tot,ref}}, \tag{9}$$

where $E_{tot,ref} = E_{tot}(\alpha = 0)$. The case with $\alpha = 0$ will therefore show 0% fuel reduction whereas the other cases will be consuming less fuel compared to this reference.

III. Results

Power profiles simulated for a specific day are shown in Fig. 3 for the case using the forecasts from the sky-imager. Compared to the load (blue dashed line), the system is most of the time overproducing the needed power (black line), with a relative mean bias error of 12.6% for the entire simulated time-period. A few blackouts occur (see e.g. before 06:00 UTC), mostly when previous long-lasting clear skies are followed by sharp cloud events. This creates a situation where the spinning reserve is too low to rapidly compensate the missing power needed to balance the demand load. Overall, at most, 4 of the 15 gensets are switched off at the same time over the entire time-period investigated. This is mostly due to the peak limiting effect of the PV system for which the total nominal power when delivering no power can only be compensated by a maximum of 5 generators at the same time, i.e. $P_{PV,nom}/P_{gen,nom} = 5$ (where $P_{PV,nom} = 1$ MW and $P_{gen,nom} = 0.2$ MW). In Fig. 4, the dependence of the percentage of fuel consumption reduction and the percentage of blackout number on the control criteria are shown for both, the cases with and without forecasts. For the "no-forecast" cases, the fuel saving indicates a rather linear dependence on the control criterion, down to -20%, whereas the number of blackouts seems to increase exponentially, up to 16%, for $\alpha = 1$. Compared with the "no-forecast" cases, the cases with forecasts shows opposite tendencies: a strong exponential decrease of fuel consumption together with a linear increase of blackouts are observed when the forecasts are changed from a pessimistic to an optimistic control strategy. A 11% difference separates the 1% percentile forecast to the perfect forecast, suggesting that further improvements to the forecasting system can lead to a significant reduction of fuel consumption. In other words, the perfect forecast gives a target reference limit, considering that the model always accurately predicts the observed solar irradiance. Finally, Fig. 5 shows the mean percentage of overproduced power (% load balance) and fuel

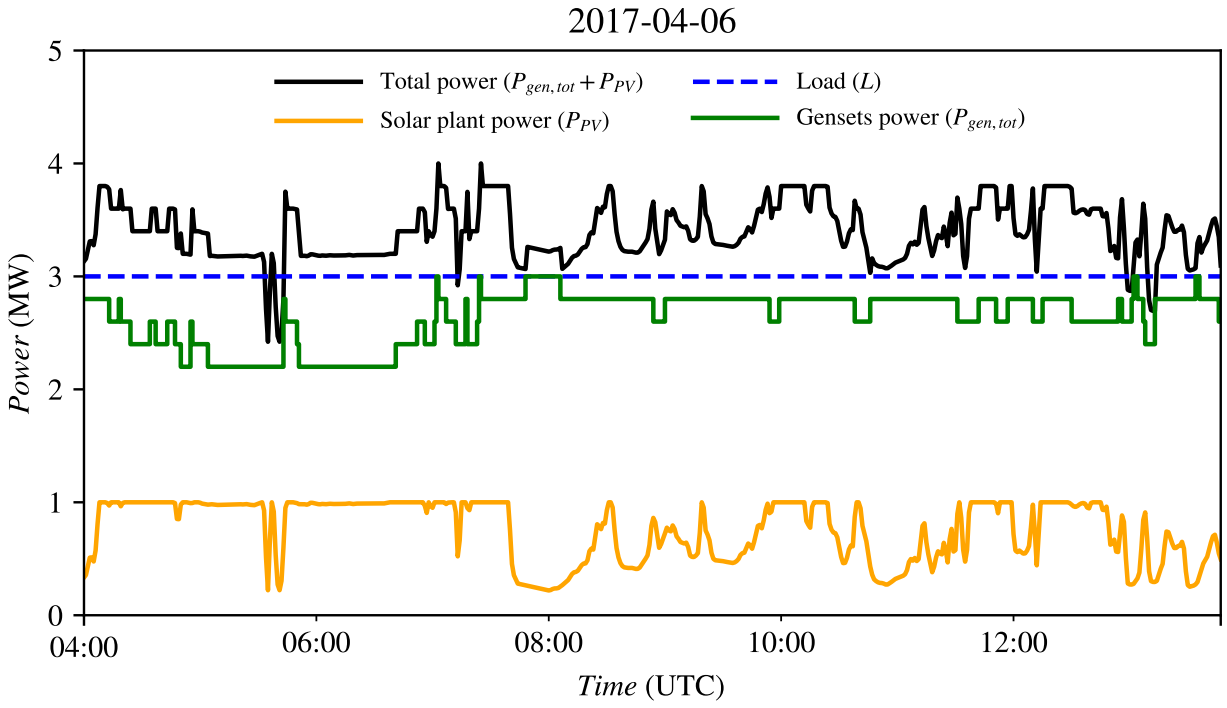

Fig. 3. Simulated power profiles of the system components on the 2017-04-06, with the gensets' control performed using the sky-imager forecasts. When the total power is below the load, a blackout occurs.

comsumption (% fuel reduction) as a function of the number of blackouts observed. The results clearly indicate a lower load balance error together with less fuel consumed for the same number of blackouts when using the forecasts, reaching down for both a 2.5% decrease for the case with 1.8% number of blackouts. This indicates that the camera forecasts can help inject more PV into the mini-grid system whereby reducing the fuel consumed from the spinning reserve of the gensets and can help diminish the potential number of blackouts.

IV. Discussion

The results indicates that the most difficult grid-management scenarios occur when long-lasting clear skies are followed by sharp cloud events. In this case, a blackout can occur as the spinning reserve of the diesel gensets is too low to rapidly compensate the sharp drop of PV power. For these situations, the forecasts help reduce the overall number of blackouts by leaving enough spin-up time to the gensets to adjust to the drastic power load balance decrease. The results also indicated that an optimal load balance control strategy can be determined to manage the risk of blackouts. Adding forecasts to this control strategy leaves even more flexibility for such management.

Our fuel consumption results are moderately better than those of previous studies [3], [4], reporting about a 2% reduction (here 2.5%) by injecting forecasts into the mini-grid system at 30% PV penetration. However, our results indicate that the fuel consumption strongly depends on the control strategy selected for injecting the PV into the grid, and on the safety criterion of demand load suppply applied (or the number of blackouts accepted). The latter can easily by eliminated, for example, by adding extra smaller fast-ramping engines ready in a few seconds to rapidly compensate the missing needed load balance at a minimal extra-fuel consumption. Additional simulations (not shown) with different numbers of gensets further showed that increasing their number helps reducing the number of blackouts by adding more flexibility to the genset system to respond accordingly to the PV variability. However, the number of generators that can be switched off to reduce the spinning reserve will always be limited by the peak limiting effect from the PV penetration. Overall, these results indicate that increasing the PV to a higher penetration level ($> 30\%$) could be safely considered if a careful design of the genset configuration is performed and if forecasts are included into the hybrid system.

However, care should be taken in generalizing these results to real-case systems as they were obtained for an idealized system with a specific plant configuration, possibly far from actual plant considerations. Especially, a variable demand load profile and diesel gensets and PV plant responses can be difficult to predict to balance an actual hybrid system. For example, the efficiencies of both the PV and diesel genset groups can vary with time due to aging, PV-plant soiling, inverters' performance, maintenance, ambient air temperature, etc. All these factors can affect the available power production ready to be delivered at a given time into the grid. Another important consideration includes the power load applied on an individual genset compared to its nominal power. In fact, the genset fuel consumption is strongly dependent on the genset optimal operating load which is usually found to be near its nominal power. Operating the gensets below this point can cause severe underperformances

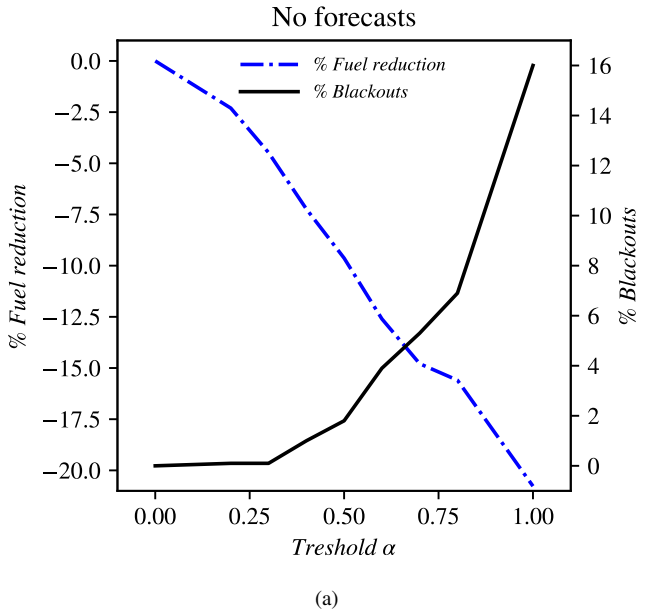

Fig. 4. Dependence of the percentage fuel reduction and percentage blackouts with the control criterion for: (a) the no forecasts approach, which varies as the control criterion α and (b) the forecasts approach, which varies as the target percentile (%). For both cases, the control scheme goes from passive to very aggressive PV injection control scenarios (from left to right on the x-axis).

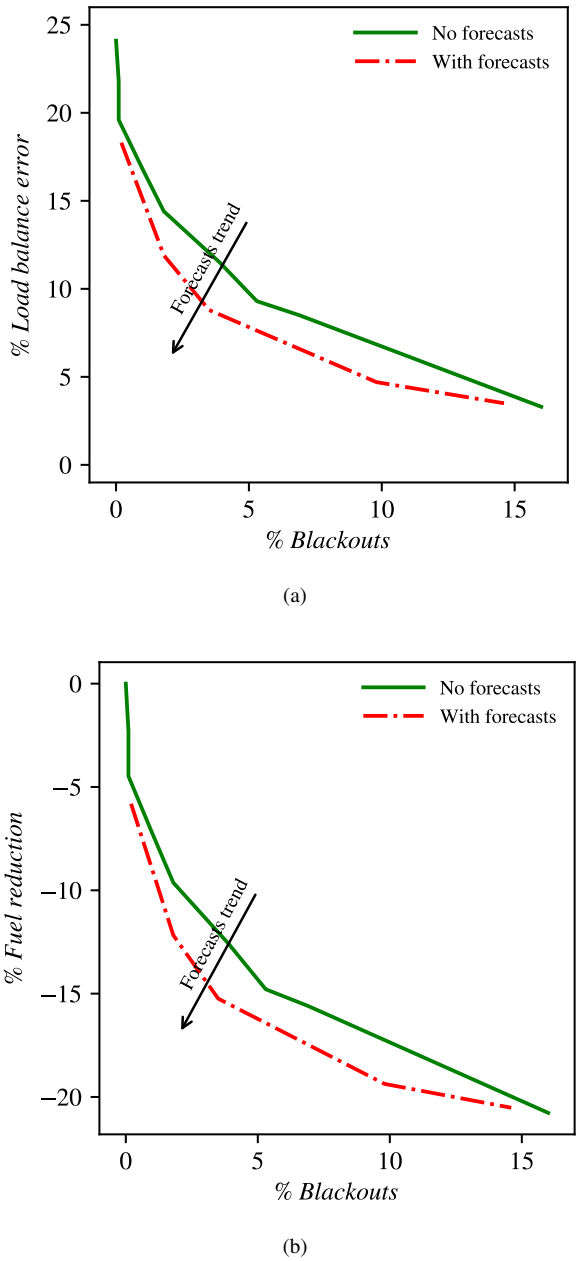

Fig. 5. Dependency of the percentage load balance (a) and percentage fuel comsumption reduction (b) on the percentage number of blackouts for the cases without forecasts (green line) compared to the cases with forecasts (red dashed line).

and a drastic increase in diesel fuel consumption, while reducing the lifecycle of the gensets. For example, running a 1 MW genset at partial load of 30% compared to 80% can double the increase of fuel consumption (from 0.2 liter/kWh to 0.4 liter/kWh, respectively), while potentially increasing the maintenance costs. In this study, we considered that the optimal operating power load of the gensets was located at their nominal power, but care should be taken to adjust their applied load to their specific optimal efficiency. As concerns the sky-imager forecasts, care should also be taken, as a forecast tailored for a given hybrid power-plant may provide different results at another site. For example, the safety level of supply needed, the local site weather and the load profile that needs to be sustained may strongly differ among the projects. Nevertheless, it was shown that the forecasts, with their relatively easy deployment and low costs, can be a cost-effective solution to manage the risks of a hybrid PV-diesel power-plant project.

V. Conclusion

Simulations were performed to investigate the benefits of including forecasts from a thermal-infrared sky-imager into an ideal hybrid PV-diesel system. The PV power output was modelled from a recorded dataset of solar irradiance and the diesel gensets were modelled as a step response after a 5-minute spin-up time. Scenarios from two approaches of

PV injection into the mini-grid system were investigated: without forecasts and with forecasts. The grid control of the cases without forecasts were based on a simple threshold criterion on the actual PV drop allowance whereas the grid control of the cases with forecasts were based on quantile predictions from a machine-learning algorithm using a thermal-infrared sky-imager system. For both approaches, passive to very agressive control strategies were simulated. Overall, the results indicated that the forecasts can add significant value by optimizing both the planification and operation phases of a hybrid solar power-plant project.

REFERENCES

[1] S.R. West, D. Rowe, S. Sayeef and A. Berry, *Short-term irradiance forecasting using skycams: Motivation and development*. Solar Energy, 110:188–207, 2014.

[2] T. Schmidt, M. Calais, E. Roy , A. Burton, D. Heinemann, T. Kilper and C. Carter, *Short-term solar forecasting based on sky images to enable higher PV generation in remote electricity networks*. Renew. Energy Environ. Sustain., 2(23), 2017.

[3] D. Peters, R. Volker, T. Kilper, M. Calais, C. Carter, T. Schmidt, K. Maydell and C. Agert, *Model based design and simulation of control strategies to maximize the PV hosting capacity in isolated diesel networks using short-term forecast for predictive control of diesel generation*, In: EUPVSEC. pp. 2532–2535, 2016.

[4] D. Peters, T. Kilper, M. Calais, T. Jamal and K. von Maydell, *Solar short-term forecasts for predictive control of battery storage capacities in remote PV diesel networks*. In: Transition Towards 100% Renewable Energy, Springer International Publishing, pp.325–333, 2018.

[5] C. Bertin, S. Cros, L. Saint-Antonin, A. and N. Schmutz, *Prediction of optical communication link availability: real-time observation of cloud patterns using a ground-based thermal infrared camera*. In: Optics in Atmospheric Propagation and Adaptive Systems XVIII, Vol. 9641, p. 96410A, 2015.

[6] G. Farneback, *Two-Frame Motion Estimation Based on Polynomial Expansion.* In: Proceedings of the 13th Scandinavian conference on Image analysis. Josef Bigun and Tomas Gustavsson (Eds.). Springer-Verlag, Berlin, Heidelberg, 2003. pp. 363–370.

[7] L. Breiman, *Random forests*. Machine Learning, 45(1):5–32, 2001.

[8] O. Liandrat, S. Cros, A. Braun, L. Saint-Antonin, J. Decroix, L. and N. Schmutz, *Cloud cover forecast from a ground-based all sky infrared thermal camera*. In: Proceedings Volume 10424 - Remote Sensing of Clouds and the Atmosphere XXII, p.104240B, 2017.

[9] C. Rigollier, O. Bauer and L. Wald, *On the clear sky model of the ESRA European Solar Radiation Atlas - with respect to the heliosat method*. Solar Energy, 68(1):33–48, 2000.